PENNSTATE

Propulsion Engineering Research Center
College of Engineering
The Pennsylvania State University
106 Research Building East — Bigler Road
University Park, PA 16802-2320

(814) 863-6272
Fax: (814) 865-3389



February 2, 1998

NASA/MSFC
Attn: COTR NA01/Uwe Hueter
Marshall Space Flight Center, AL 35812

Dear Mr. Hueter:

Enclosed is a copy of the second milestone report "Detailed Experimental Data for CFD Code Validation."

If there are any questions concerning this milestone report or its format, please contact me by phone at (814)863-1285 or by fax at (814)865-3389.

Very truly yours,

Robert J. Santoro

Robert J. Santoro
Professor of Mechanical Engineering

RJS:sp
Enclosures
cc: GP54-G (1 copy)
CN31D (3 copies)
LA10/New Technology Representative (1 copy)
Alt. COTR EE61/J. Turner (1 copy)
MSFC Lead EP61/J. Price (1 copy)
DCMAO/DPRO/ONRRR (1 copy)
NASA Center for Aerospace Information (2 copies)
S. Pal
J. Feng
P. Buelow

# DETAILED EXPERIMENTAL DATA FOR CFD CODE VALIDATION

## INTRODUCTION

Recent interest in low cost, reliable access to space has generated increased interest in advanced technology approaches to space transportation systems. A key to the success of such programs lies in the development of advanced propulsion systems capable of achieving the performance and operations goals required for the next generation of space vehicles. One extremely promising approach involves the combination of rocket and air-breathing engines into a rocket-based combined-cycle engine (RBCC). A key element of that engine is the rocket ejector that is utilized in the zero to Mach two operating regime. Studies of RBCC engine concepts are not new and studies dating back thirty years are well documented in the literature. However, studies focused on the rocket ejector mode of the RBCC cycle are lacking. The present investigation utilizes an integrated experimental and computation fluid dynamics (CFD) approach to examine critical rocket ejector performance issues. In particular, the development of a predictive methodology capable of performance prediction is a key objective in order to analyze thermal choking and its control, primary/secondary pressure matching considerations, and effects of nozzle expansion ratio. To achieve this objective, the present study emphasizes obtaining new data using advanced optical diagnostics such as Schlieren photography and Raman spectroscopy, and CFD techniques to investigate mixing in the rocket ejector mode. A new research facility for the study of the rocket ejector mode has been developed. In the last milestone report, the operational capabilities of this research facility were described. In this milestone report, the experimentally obtained measurements for CFD code validation are presented and discussed.

## EXPERIMENTAL APPROACH

The current experimental configuration is based on the well-known 1968 experimental rocket-ejector study of Odegaard and Stroup [1]. It is recognized that advancements of both proprietary and classified natures have been made in the last thirty years, however, this particular geometry is chosen as the baseline configuration because it represents the most comprehensive set of data available in the open literature. The scope of the current study is not to simply duplicate the experiments of Odegaard and Stroup, but to build on this study by bringing to bear

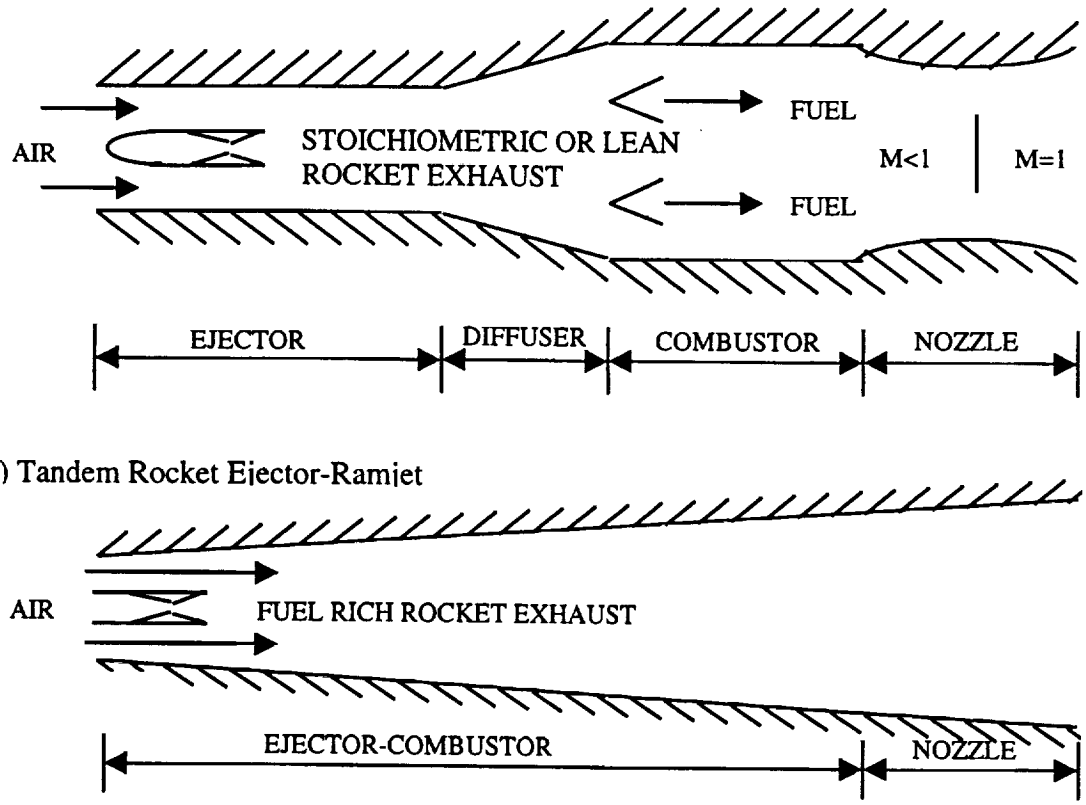


**Fig. 1.** Basic Ejector cycles described by Billig (1993).

advances made in both diagnostic and analytical techniques to qualitatively document the flow characteristics of the rocket-ejector mode of the RBCC engine.

From an RBCC engine design point-of-view, two basic ejector cycles are potentially attractive as noted by Billig [2] and schematized in Fig. 1. The first cycle concept includes a sequential inlet/rocket ejector/mixer/diffuser/combustor/nozzle assembly. This is also the cycle that was studied by Odegaard and Stroup. The second cycle concept features a single integrated duct with no physical nozzle that counts on thermal choke to simulate the key features of the first cycle. The current experimental configuration is designed such that both cycle concepts can be investigated.

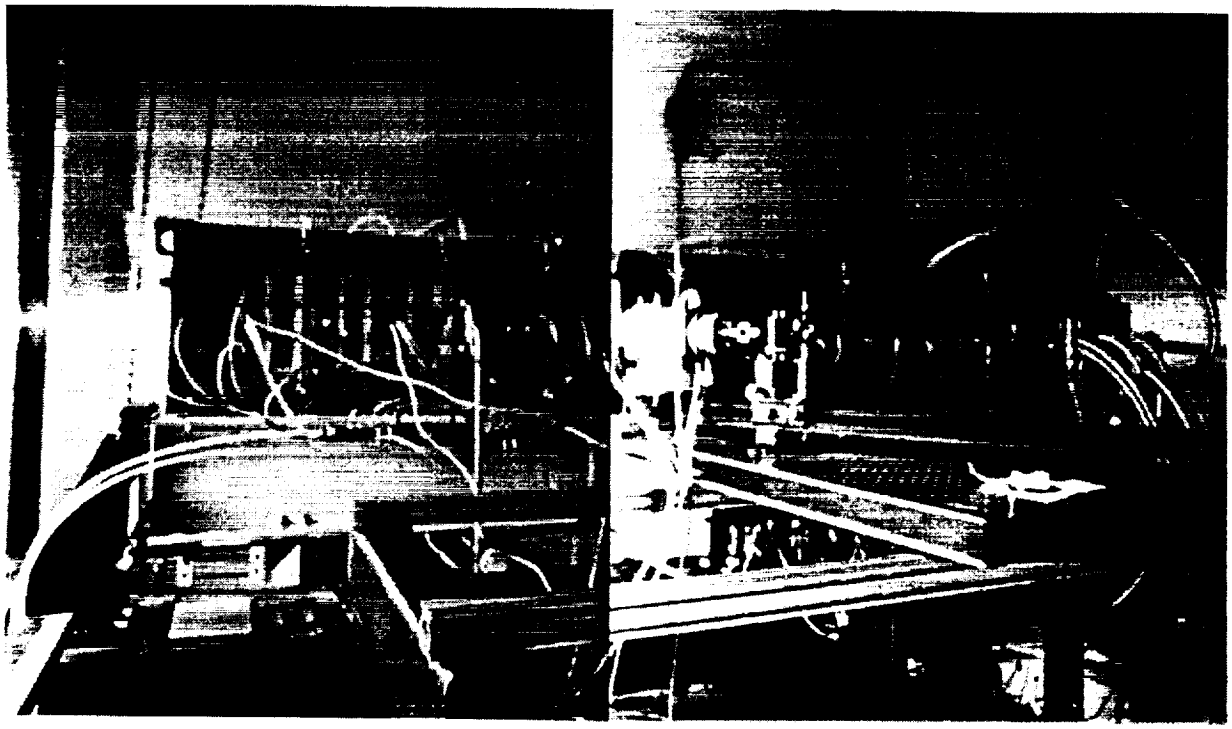

**Fig. 2.** Photograph of rocket-ejector firing. Flow is from right to left. The rocket can be seen on the extreme right hand side of the rocker-ejector hardware. For this photograph, the afterburner was operational. The rocket-ejector exhaust plume can be seen in the photograph. Part of the Schlieren system (camera side) used for qualitative characterization of the rocket exhaust/air stream mixing is also seen in the photograph.

In this milestone report, the rocket-ejector system corresponding to the first cycle concept is described first. This description is followed by a presentation of the experimental results obtained for CFD code validation.

## ROCKET-EJECTOR SYSTEM

A low-cost modular single rocket based optically-accessible rocket-ejector system that duplicates the important physical parameters of the Odegaard and Stroup [1] experimental setup has been designed and fabricated. The design stresses modularity for studying the important effects of thermal choking, preferred nozzle primary area ratios and primary-secondary pressure matching. The rocket ejector is designed as a two-dimensional system. A photograph of the rocket-ejector system firing is shown in Fig. 2. The two-dimensionality of the system enables the easy change of the primary rocket's gaseous oxygen/hydrogen injector geometry and nozzle throat to exit area ratio and the ejector/ramjet's mixer length, diffuser length and angle, ramjet

**Table 1.** Comparison between Odegaard and Stroup [1] ERJ engine and PSU version.

| Odegaard and Stroup [1] ERJ Engine | PSU version |
|---|---|
| **Inlet Geometry** | |
| **Inlet** | **Inlet** |
| (1) Bell Mouth 1 (9.2 in. for Sea Level) | (1) Bell Mouth 1 (2.89 x 3.0 in.; Rectangular) |
| (2) Normal Shock (7.2 in. Cowl Diameter for Mach 1) | (2) Normal Shock (1.77 x 3.0 in.; Rectangular) |
| (3) Normal Shock (8.2 in. Cowl Diameter for Mach 1.9) | (3) Normal Shock (2.30 x 3.0 in.; Rectangular) |
| *Note: Mach 1 @ 9,000 ft; T=270 K; P=10.5 psia*<br>*Mach 1.9 @40,000 ft; T=218 K; P=2.72 psia* | *Note: Sized inlet based on area ratio for one primary rocket (rectangular).*<br>*Direct Connect; Air Supplied Corresponding to Above Conditions* |
| **Primary Rockets** | |
| **Primary Rockets (8)** | **Primary Rocket (1)** |
| $GO_2/GH_2$ Combustion; O/F = 7.94 | $GO_2/GH_2$ Combustion; O/F = 8.0 |
| Diameter of throat (1)= 0.59 in. | Rectangular throat = 0.1 x 3.0 in. |
| Nozzle area ratio=6 | Nozzle area ratio=6 |
| Diameter of nozzle exit (1)= 1.446 in. | Rectangular nozzle exit = 0.6 x 3.0 in. |
| $GH_2$ Mass flowrate (1)=6.88 x $10^{-2}$ lbm/s | $GH_2$ Mass flowrate=0.075 lbm/s |
| $GO_2$ Mass flowrate (1)=5.47 x $10^{-1}$ lbm/s | $GO_2$ Mass flowrate=0.60 lbm/s |
| $P_o$=500 psia | $P_o$=500 psia |
| Rocket external diameter == 2 in. | External cross section of rocket 1.75 x 3.0 in. |
| Duct diameter = 12 in. | Duct cross section=5.0 x 3.0 in. |
| **Mixer/Diffuser Sections** | |
| **Mixer Section** | **Mixer Section** |
| Constant diameter mixer section = 12 in. | Constant rect. mixer section = 5.0 x 3.0 in. |
| L= 0, 14.0, 36.0, 54.0 in. | L= 0, 14.0, 35.0 in. |
| | *Note: Lengths are conserved; sector argument* |
| **Diffuser Section** | **Diffuser Section** |
| Inlet diameter = 12 in. | Inlet cross section=5.0 x 3.0 in. |
| Outlet diameter = 18 in. | Outlet cross section=10.0 x 3.0 in. (ADJUSTABLE) |
| Half angles of 5° (L=34.3 in.) and 12° (L=14.1 in.) | Lengths of 35.0 and 14.0 in.<br>*Note: Lengths are conserved; sector argument* |
| **Afterburner/Nozzle Sections** | |
| **Fuel Injectors** | **Fuel Injectors** |
| 24 finger (4.5 and 7 in.) type radials<br>Injection near diffuser exit @ 17 in. diameter location | Injector design is similar to Odegaard and Stroup [1] injectors. |
| **Afterburner** | **Afterburner** |
| Afterburner diameter = 18 in. | Afterburner area = 10.0 x 3.0 in. (ADJUSTABLE) |
| Design Equivalence Ratio = 1.0 | Design Equivalence Ratio = 1.0 |
| L/D= 1.0 | Length of 18 in. |
| **Exit Nozzles** | **Exit Nozzles** |
| Convergent;: Exit diameters of 14.3 and 12.1 in. | Convergent: Exit areas of 7.0 x 3.0 in. and 5.0 x 3.0 in. (ADJUSTABLE) |
| Convergent/Divergent: Throat diameter of 13.8 in. | Convergent/Divergent: Throat area of 6.5 x 3.0 in. (ADJUSTABLE) |

injectors, afterburner length and exit nozzle geometry. This design flexibility is necessary for optimizing the overall geometry of the system for maximum performance, a feature not available in the fixed geometry system tested by Odegaard and Stroup. The key geometric/flow parameters defining the current two-dimensional rocket-ejector system are directly based on the earlier study as summarized in Table 1.

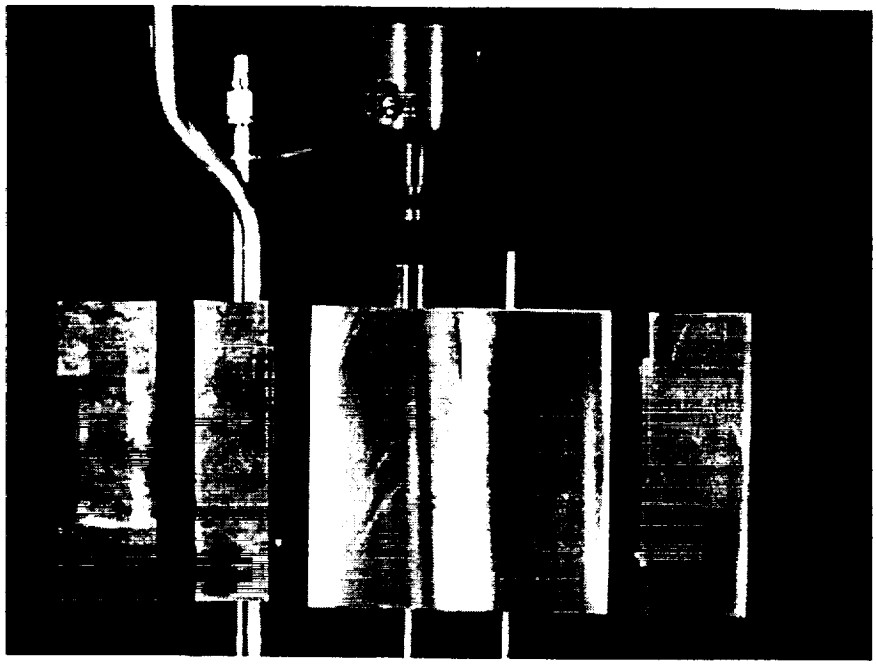

**Fig. 3.** Photograph of the assembled rectangular rocker chamber. From left to right, a) Elliptical nose cone, b) planar O-F-O triplet injector, c) rectangular cross-section rocket chamber shown with ignitor and d) nozzle section.

The inlet geometry of the ejector ramjet involves direct connect for free jet testing at simulated conditions of Mach 1 at 9400 ft and Mach 1.9 at 40,000 ft for a nominal 1000 psf dynamic pressure trajectory. These conditions are the same as those tested in the earlier study.

The single primary $GO_2/GH_2$ rocket is designed similar to one of the eight primary rockets in the Odegaard and Stroup hardware for stoichiometric operation at a maximum chamber pressure of 500 psia. A photograph of the rocket assembly is shown in Fig. 3. Experiments at both stoichiometric and fuel-rich conditions have been carried out. The fuel-rich operation of the rocket was carried out to investigate the possibility of not using the ramjet $GH_2$ injectors. For the Odegaard and Stroup experiments, low c* efficiencies for the primary rocket affected the overall performance of the rocket ejector system. The present rocket injector design features a planar version of a demonstrated high mixing and combustion efficiency O-F-O triplet injector. This injector geometry has been demonstrated to yield high c* efficiencies.

The mixer and diffuser sections are designed to scale with the complementary Odegaard and Stroup design parameters but benefit from the two-dimensionality of the system in that the mixer length and diffuser length and angle are variable such that the overall system can be

optimized for performance. Optical access in both the mixer and diffuser sections enables the application of non-intrusive laser-based diagnostics.

The final two components, the afterburner and the nozzle, are also designed to scale with the earlier setup with the same added features of adjustable afterburner length and nozzle convergence angle and throat area. The afterburner also has optical access for diagnostic application.

The rocket-ejector system is mounted on a thrust cell for thrust measurements and is instrumented with numerous static pressure ports on all walls and heat flux gauges.

### NEW TEST FACILITY

The rocket-ejector system is operational in the recently upgraded test facility at the Cryogenic Combustion Laboratory (CCL) at the Propulsion Engineering Research Center. The CCL now features two testing areas, the first for rocket experiments and the second new area dedicated for RBCC experiments. The maximum air, gaseous oxygen and gaseous hydrogen flowrate capabilities of the facility are 5, 1 and 0.25 lbm/s, respectively. For the air-augmented rocket ejector experiments discussed here, the flowrate capabilities of the laboratory well exceed the requirements.

### ADVANCED DIAGNOSTIC TECHNIQUES

The fluid dynamic processes within the rocket-ejector system were characterized by Schlieren photography. The results obtained using Schlieren photography are described later in this milestone report. Schlieren photography provides information on the mixing between the rocket exhaust and the air stream within the system.

## EXPERIMENTAL RESULTS

The first set of experiments described here was conducted for the flow conditions shown in Table 2. Experiments for both stoichiometric rocket/afterburner and fuel-rich rocket/no afterburner were conducted for a rocket operating pressure of 200 psia. In Table 2, for cases 1 and 2, the operating mixture ratio of the rocket was four. The two cases differ in the amount of air introduced into the system. For case 1, the excess hydrogen in the rocket plume depletes the oxygen in the air stream, whereas for Case 2, the airflow is defined such that the oxygen in the air can burn stoichiometrically with the excess hydrogen in the rocket exhaust. For these two cases,

**Table 2.** Target Flow Conditions for Initial Experiments.

| | CASE 1 | CASE 2 | CASE 3 | CASE 4 |
|---|---|---|---|---|
| **Rocket** | | | | |
| O/F | 4 | 4 | 8 | 8 |
| $GO_2$ flow (lbm/s) | 0.188 | 0.188 | 0.243 | 0.243 |
| $GH_2$ flow (lbm/s) | 0.047 | 0.047 | 0.030 | 0.030 |
| $P_C$ (psia) | 200 | 200 | 200 | 200 |
| **Duct** | | | | |
| Air flow (lbm/s) | 0.63 | 0.81 | 0.63 | 0.81 |
| $GH_2$ flow in afterburner (lbm/s) | 0 | 0 | 0.018 | 0.024 |
| Air flow/Total Rocket Flow | 2.68 | 3.43 | 2.30 | 2.95 |
| Excess $GH_2$ in rocket exhaust (lbm/s) | 0.024 | 0.024 | 0 | 0 |
| $GO_2$ in air stream (lbm/s) | 0.147 | 0.188 | 0.147 | 0.1880 |
| O/F between $GO_2$ in air and $GH_2$ (in duct) | 6.25 | 8 | 8 | 8 |

there is no downstream introduction of gaseous hydrogen. For cases 3 and 4, the operating gaseous oxygen/gaseous hydrogen mixture ratio was stoichiometric. The two conditions differ in the amount of introduced air, and therefore bypass ratio. For these two cases, the afterburner was operational, with the amount of injected gaseous hydrogen set to burn stoichiometrically with the oxygen in the air stream. For the sake of completeness, experiments for cases 3 and 4 were also conducted with the gaseous hydrogen flow turned off in the afterburner. The hydrogen for the afterburner is introduced through a set of equally spaced straight orifices on both side walls that are located at the end of the diffuser section.

For each flow condition, the air duct static pressure distribution, wall heat flux distribution and overall rocket-ejector thrust were measured. Schlieren photography was utilized to characterize the flowfield for all flow conditions. In the following discussion, each set of results is presented individually.

## STATIC PRESSURE MEASUREMENTS

The static pressure profiles in the duct for all flow conditions were measured with top and side wall mounted pressure ports. The pressure was sampled at 200 Hz for the duration of the two (or four) second firings. The time trace of each pressure measurement indicated that steady state pressure conditions was attained. The axial pressure profiles for cases 1-3 are plotted in

Fig. 4. In the figure, the schematic of the rocket-ejector system is drawn to scale on the top for direct reference. The results indicate that for all flow condition the static pressure at a give axial location is nominally the same irrespective of whether the pressure was measured on the side or top wall. This observation leads credence to the notion that one-dimensional analysis can be used to at least address the global characteristics of the flowfield. As is evident, for any given flow condition, the static pressure is lowest in the region occupied by the rocket, increases both in the mixer and diffuser sections, is nearly constant in the afterburner and finally decreases to match atmospheric pressure at the end of the nozzle.

## HEAT FLUX MEASUREMENTS

The measured heat flux profiles are shown in Fig. 5 for cases 1-4. In the figure, the rocket-ejector system is again shown for reference. The heat flux at a given axial location was measured with the use of 0.5 in. diameter Gardon heat flux gauges mounted on the side wall along the central axis of the rocket-ejector system. The measurements were sampled at 200 Hz. Since the rocket exhaust grazes the side walls along the central axis of the rocket-ejector system as it mixes with the cold air from the top and bottom, it is expected that close to the rocket exhaust, the heat flux can not be treated as one-dimensional. The measurements shown in Fig. 5 therefore represent the highest heat flux at an axial location. This statement is also verified by inspection of the inside surface of the blank copper window blanks that indicate discoloration along the central axis (indicating higher heat flux). The axial heat flux profiles for all tested cases show maximum heat flux at the nozzle exit. As expected, the heat flux levels decrease rapidly with downstream distance. Comparison of the heat flux levels for cases where the rocket operates at a mixture ratio of four (cases 1 and 2) with the stoichiometric rocket cases (cases 3 and 4) shows higher levels of heat flux near the rocket exhaust region for cases where the rocket mixture ratio is four. The mean temperature of the flowfield downstream of the rocket clearly decreases with axial distance for the stoichiometric rocket case due to mixing with the cold air. However, for the fuel-rich cases of mixture ratio of four, the excess hydrogen in the rocket plume combusts with air in the mixer section and consequently the temperature is higher than that of the stoichiometric case. The higher heat flux level noted in Fig. 5 for the fuel-rich rocket cases is attributed to the aforementioned reasoning.

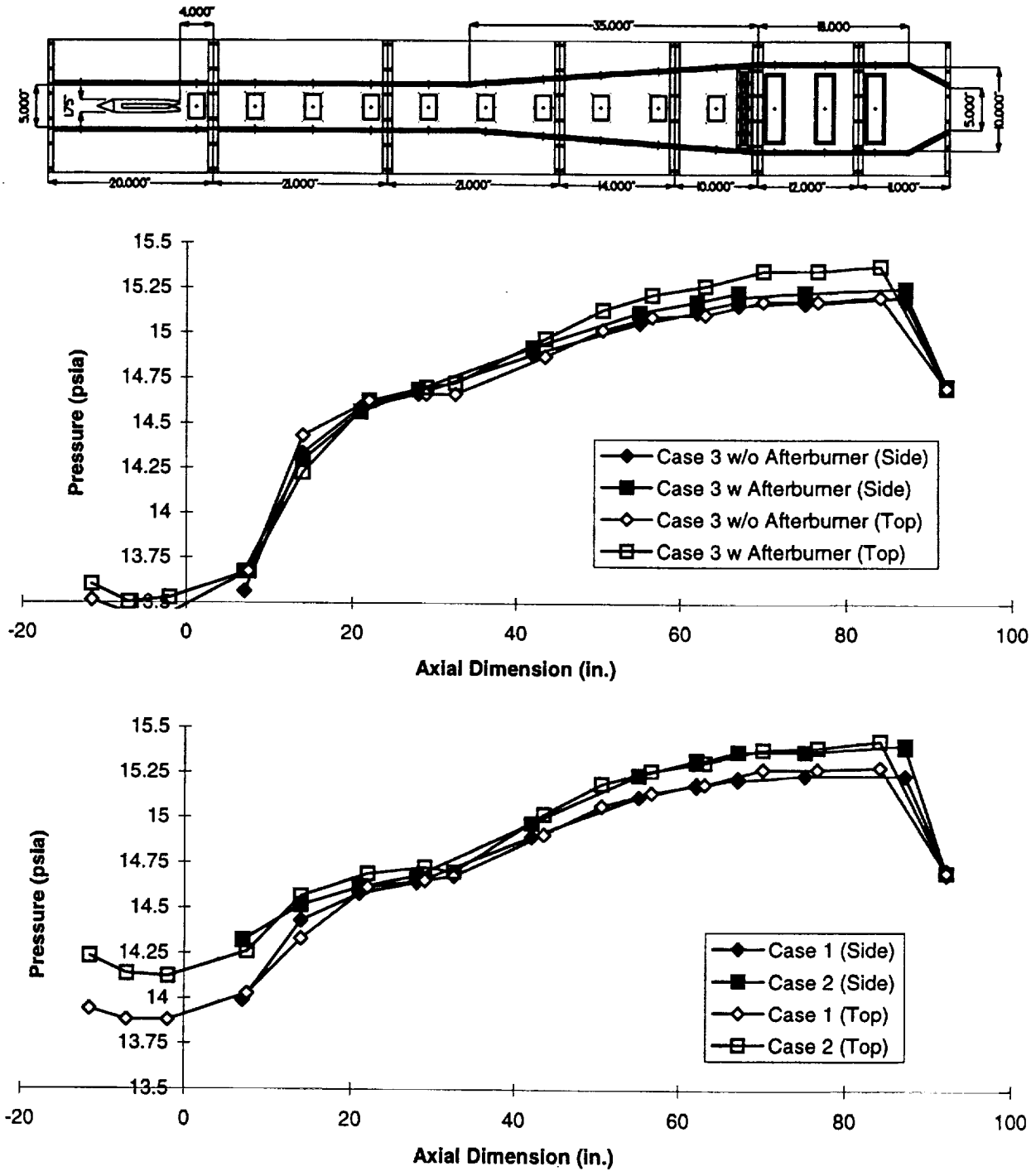


**Fig. 4.** Static pressure versus axial dimension along rocket-ejector. See Table 2 for flow conditions. "Side" and "top" refer to pressure taps located on the side and top walls, respectively. The scale of the abscissa for the static pressure profiles corresponds to the scale of the rocket ejector schematic shown on the top.

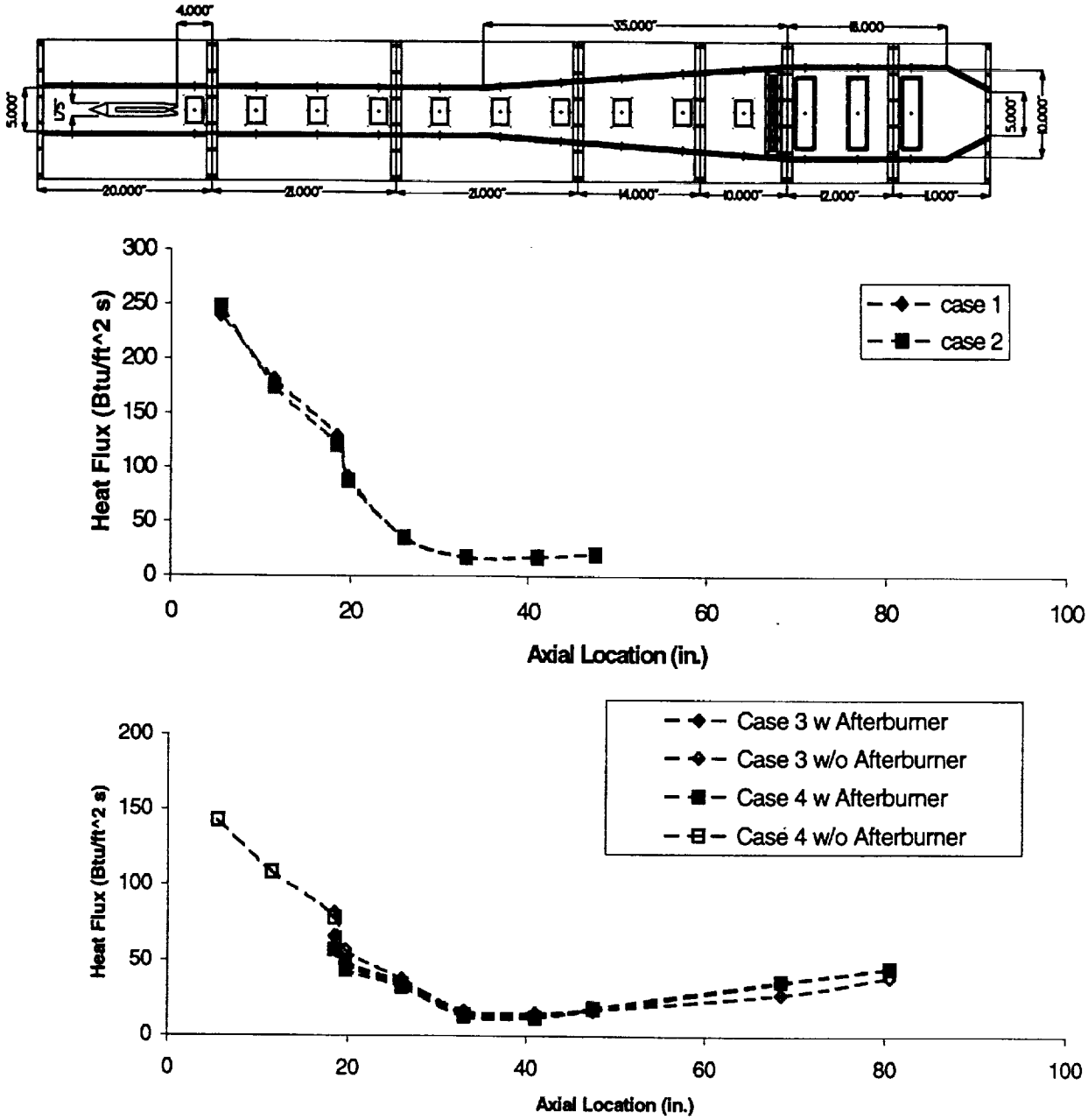


**Fig. 5.** Heat flux versus axial dimension along rocket-ejector. See Table 2 for flow conditions. The heat flux gauges were mounted on the centerline of the side wall. The scale of the abscissa for the heat flux profiles corresponds to the scale of the rocket ejector schematic shown on the top.

## ROCKET-EJECTOR THRUST MEASUREMENTS

Representative thrust versus time plots for each of the four rocket-ejector firing cases are shown in Fig. 6. The actual firing starts at about 3.25 s and lasts up to about 5.25 s on the time scale shown (2 s firing). The thrust versus time history shows a "noisy" signal before the test and during the startup portion of the firing. This "noise" is electric noise from the spark source used for igniting the propellants in the ignitor. Aside from this noise, the thrust is seen to be constant during the steady state portion of the firing. The thrust achieved for the four cases is nominally between 35 and 45 lbf. The results show that the thrust is slightly higher for the stoichiometric rocket cases (cases 3 and 4). As evident from the figures, steady state conditions within the rocket-ejector system is achieved in a very short duration (< 0.5 s). The Schlieren photographs described in the next section were taken during the steady-state portion of the firings.

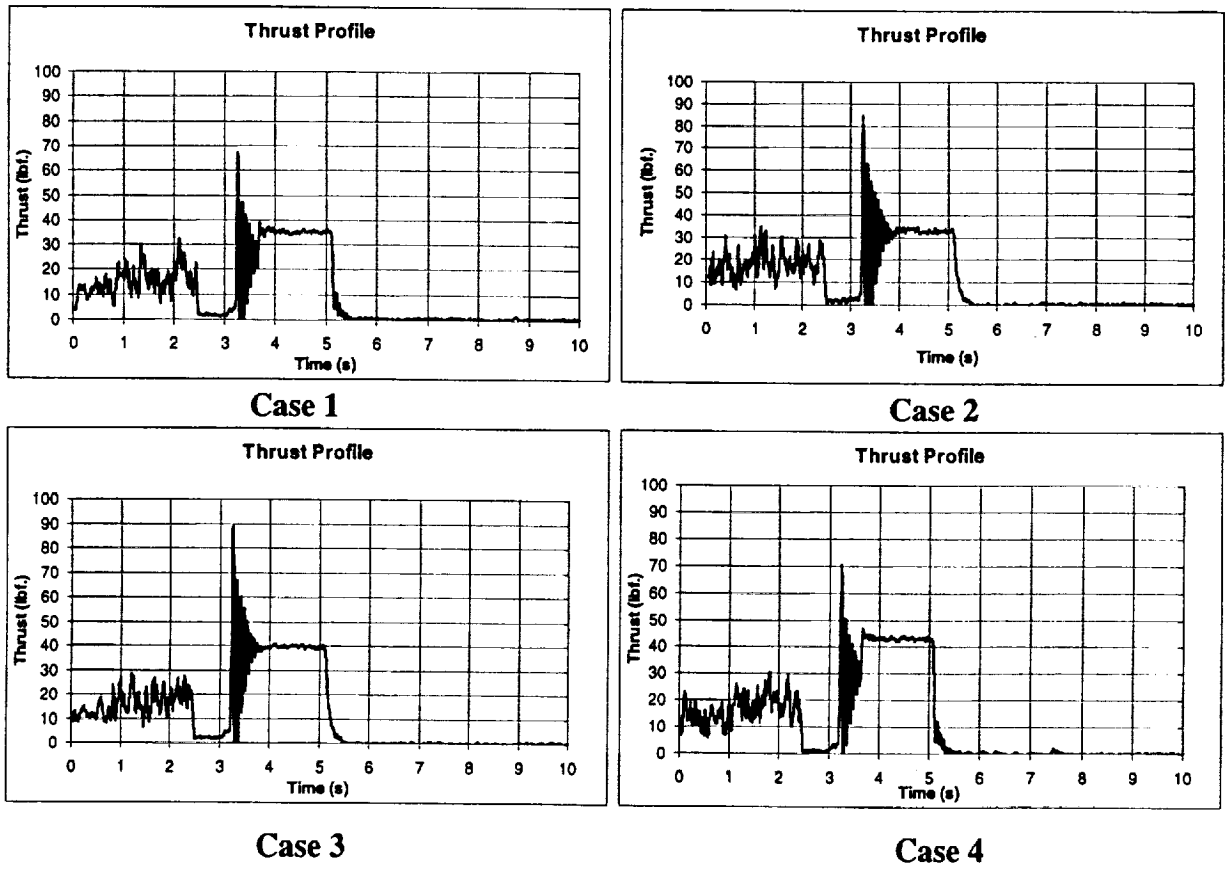


**Fig. 6.** Thrust versus time for rocket-ejector firings. Flow conditions for each case number are tabulated in Table 2. Note that the noise on the graphs during startup are due to electric noise interference from the ignition source. The measurements show that thrust is constant during the steady-state portion of each firing.

## SCHLIEREN CHARACTERIZATION OF FLOWFIELD

The flowfield downstream of the rocket exit plane was also qualitatively characterized using Schlieren photography. In Figs. 7 and 8, two Schlieren images corresponding to Cases 1 and 4 (see Table 2 for flow conditions) are shown. In each figure, the image on the right was taken at the first window location downstream of the rocket exit plane (see schematic in Figs. 4 or 5), whereas the image on the left corresponds to the second window location. Note that 2 in. diameter, 1 in. thick circular quartz windows placed in appropriate flanges were placed in the rectangular window section for these photographs. Previous experience has shown that circular windows are more amenable to high temperature environments than rectangular windows, and hence as a precaution, this hardware change was exercised for the window locations close to the rocket exhaust.

The image close to the rocket nozzle exit plane (axial field of view of 1.5-3.5 in.) clearly shows the rocket exhaust plume. Note that Schlieren images represent density gradients and not

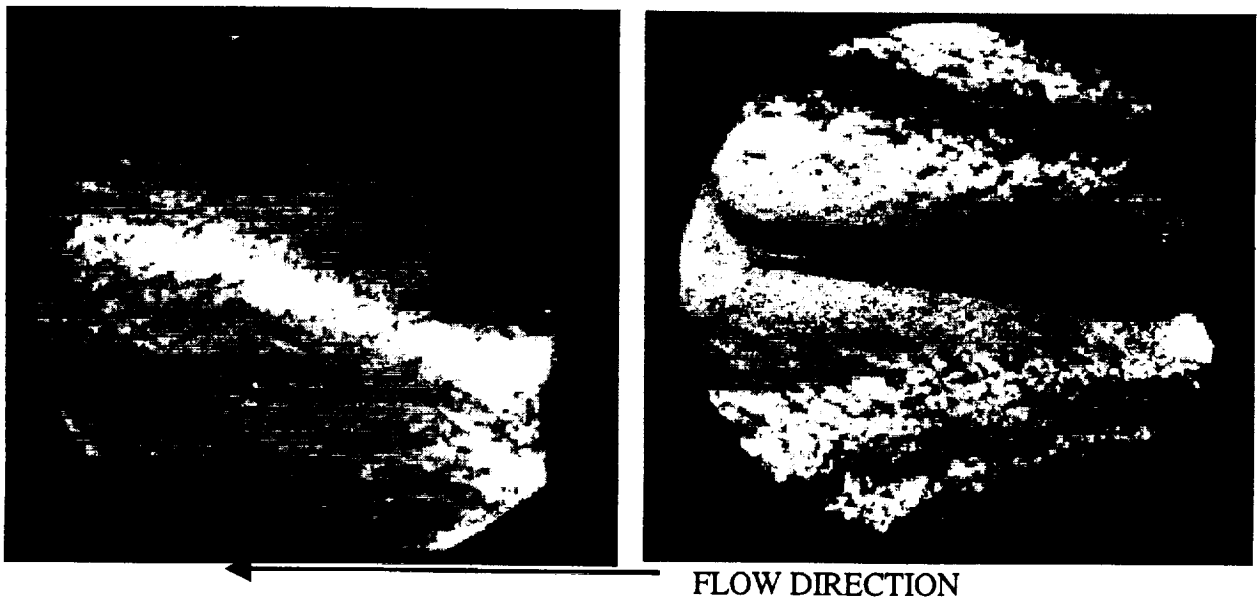


**Fig. 7.** Schlieren images showing the mixing between the rocket exhaust and the air stream in the rocket-ejector system. The flow conditions correspond to case 1 in Table 2. For reference on window locations, see schematic on Figure 4. Image on right is at the first window location (field of view is 1.5-3.5 in.), whereas the image on the left is at the second window location (field of view is 8.5-10.5 in.). The corresponding image at the third window location (not shown here; field of view from 15.5-17.5 in.) shows no "Schlieren" structures suggesting that mixing is complete. These qualitative images indicate that for the flow conditions of these experiments, mixing is complete between the second and third window locations.

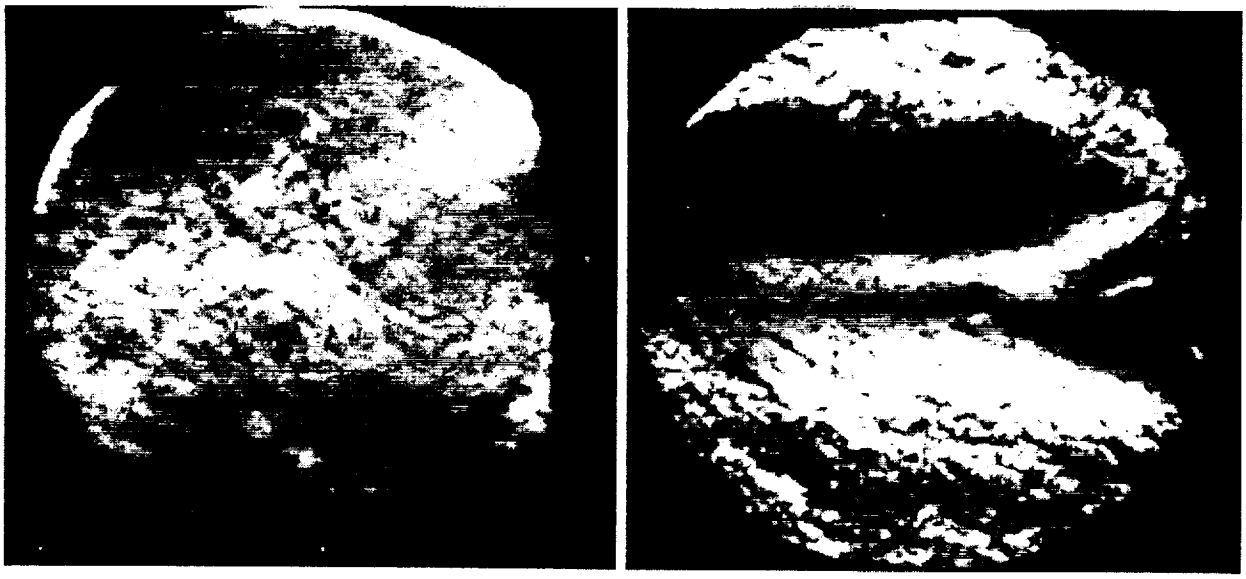


**Fig. 8.** Schlieren images showing the mixing between the rocket exhaust and the air stream in the rocket-ejector system. The flow conditions correspond to case 4 in Table 2. The comments in the caption for Fig. 7 also apply to this figure.

absolute density, and hence, the coloration is asymmetric around the central axis. At the second location with an axial field of view of 8.5-10.5 in., the observed density gradients are more gradual and spread out over the viewing area. The image indicates that up to this axial location, mixing between the rocket exhaust and air stream is not complete. A similar Schlieren image taken at the third window location (not shown here; axial extent of 15.5-17.5 in.) shows no "Schlieren" structures indicating that the flowfield has more or less a uniform density. The mixing process is therefore completed somewhere between the second and third window locations. These qualitative images indicate that if the rocket nozzle exit height of 0.6 in. is taken as a characteristic length scale, mixing is complete between 17.5 and 26 length to nozzle exit height ratio. Similar results and conclusions were also obtained for the other two flow conditions for which images are not presented here.

## SUMMARY

A new test facility has been constructed for experimentation of a two-dimensional, variable-geometry flow-path rocket-ejector system for an RBCC engine. The first phase of experimentation to obtain experimental data for CFD code validation has been completed.

## REFERENCES

[1] Odegaard, E. A. and Stroup, K. E., "1966 Advanced Ramjet Concepts program, Volume VIII-Ejector Ramjet Engine Tests- Phase I" The Marquardt Corporation, Technical Report AFAPL-TR-67-118 Volume VIII, January 1968.

[2] Billig, F. S., "Advanced Propulsion Technology Program, SSTO Low Speed System Assessment Final Report," The Johns Hopkins University Applied Physics Laboratory, JHU/APL AL-95-A050, June 1995.